Incommensurate and commensurate antiferromagnetic states in $CaMn_2As_2$ and $SrMn_2As_2$ revealed by ^{75}As NMR

Q.-P. Ding [1,2] N. S. Sangeetha,[1,*] Abhishek Pandey [1,†] D. C. Johnston [1,2] and Y. Furukawa [1,2]
[1]*Ames Laboratory, Iowa State University, Ames, Iowa 50011, USA*
[2]*Department of Physics and Astronomy, Iowa State University, Ames, Iowa 50011, USA*

(Received 22 September 2021; revised 22 November 2021; accepted 30 November 2021; published 9 December 2021)

We carried out ^{75}As nuclear magnetic resonance (NMR) measurements on the trigonal $CaMn_2As_2$ and $SrMn_2As_2$ insulators exhibiting antiferromagnetic (AFM) ordered states below Néel temperatures $T_N = 62$ and 120 K, respectively. In the paramagnetic state above T_N, typical quadrupolar-split ^{75}As NMR spectra were observed for both systems. The ^{75}As quadrupolar frequency ν_Q for $CaMn_2As_2$ decreases with decreasing temperature, while ν_Q for $SrMn_2As_2$ increases, showing an opposite temperature dependence. In the AFM state, the relatively sharp and distinct ^{75}As NMR lines were observed in $SrMn_2As_2$ and the NMR spectra were shifted to lower fields for both magnetic fields $H \parallel c$ axis and $H \parallel ab$ plane, suggesting that the internal fields B_{int} at the As site produced by the Mn ordered moments are nearly perpendicular to the external magnetic field direction. No obvious distribution of B_{int} was observed in $SrMn_2As_2$, which clearly indicates a commensurate AFM state. In sharp contrast to $SrMn_2As_2$, broad and complex NMR spectra were observed in $CaMn_2As_2$ in the AFM state, which clearly shows a distribution of B_{int} at the As site, indicating an incommensurate state. From the analysis of the characteristic shape of the observed spectra, the AFM state of $CaMn_2As_2$ was determined to be a two-dimensional incommensurate state where Mn ordered moments are aligned in the *ab* plane. A possible origin for the different AFM states in the systems was discussed. Both $CaMn_2As_2$ and $SrMn_2As_2$ show very large anisotropy in the nuclear spin-lattice relaxation rate $1/T_1$ in the paramagnetic state. $1/T_1$ for $H \parallel ab$ is much larger than that for $H \parallel c$, indicating strong anisotropic AFM spin fluctuations in both compounds.

DOI: 10.1103/PhysRevB.104.224413

I. INTRODUCTION

After the discovery of superconductivity (SC) in iron-based pnictides in 2008 [1], considerable experimental and theoretical attention has concentrated on transition-metal pnictides [2–4]. Among them, the Mn compounds have been found to show a rich variety of magnetic properties with different crystal structures. $BaMn_2As_2$ with the body-centered tetragonal $ThCr_2Si_2$-type structure (space group $I4/mmm$), similar to the parent compound $BaFe_2As_2$, is a G-type collinear antiferromagnet with a Néel temperature of 625 K where the ordered Mn moments aligned along the tetragonal c axis [5]. On the other hand, (Ca, Sr)Mn_2P_2 [6,7], (Ca, Sr)Mn_2As_2 [6,8–10], (Ca, Sr)Mn_2Sb_2 [11–13], and $CaMn_2Bi_2$ [14] crystallize in the trigonal $CaAl_2Si_2$-type structure (space group $P\bar{3}m1$) shown in Fig. 1(a) where the Mn ions form a triangular lattice bilayer which can be considered as a corrugated Mn honeycomb sublattice [see Fig. 1(b)] [14]. The honeycomb lattice structure is interesting as a spin system with spin frustration originating from competing interactions [15–17]. Interestingly, recent theoretical studies and density-functional theory calculations have suggested that the $CaAl_2Si_2$-type transition-metal pnictides might comprise a new family of magnetically frustrated materials to study the potential superconducting mechanism [18,19].

Magnetic susceptibility (χ), electrical resistivity, and heat capacity measurements revealed that $CaMn_2As_2$ and $SrMn_2As_2$ are antiferromagnetic (AFM) insulators with $T_N = 62(3)$ K and $T_N = 120(2)$ K, respectively [10]. In the AFM state, χ is nearly independent of temperature T for magnetic fields $H \parallel c$ axis, while χ for $H \parallel ab$ plane decreases with decreasing temperature, indicating that the hexagonal c axis is the hard axis and hence that the ordered Mn moments are aligned in the *ab* plane. However, χ_{ab} does not go to zero at low T but attains a value $\chi_{ab}(T \to 0) \simeq 0.6\ \chi_c(T_N)$, in contrast to the case of a simple collinear antiferromagnet with H parallel to the ordering axis where $\chi_{ab}(T \to 0) \to 0$. If H is perpendicular to the ordering axis, then $\chi_{ab}(T \to 0) \sim \chi_{ab}(T_N)$ [20,21]. This suggests that the AFM structure could be either a collinear antiferromagnet with multiple domains aligned within the *ab* plane or an intrinsic noncollinear structure with moments again aligned in the *ab* plane [20–23]. Subsequent single-crystal neutron-diffraction measurements on $SrMn_2As_2$ clearly demonstrated that the Mn moments ($3.6\mu_B$ at $T = 5$ K) are ordered in a collinear Néel AFM phase with 180° AFM alignment between a moment and all nearest-neighbor moments in the basal plane and also perpendicular to it [see Fig. 1(b)] [24]. Therefore, in order to explain the finite $\chi_{ab}(T \to 0)$, an occurrence of multiple AFM domains is suggested in $SrMn_2As_2$ [10,24]. For $CaMn_2As_2$, the AFM magnetic structure has not been determined yet.

*Present address: Institute for Experimental Physics IV, Ruhr University Bochum, 44801 Bochum, Germany.
†Present address: School of Physics, University of the Witwatersrand, Johannesburg, Gauteng 2050, South Africa.

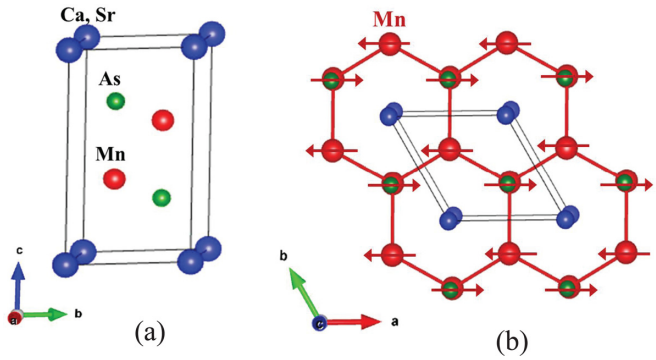

FIG. 1. Trigonal $CaAl_2Si_2$-type crystal structure of $CaMn_2As_2$ and $SrMn_2As_2$ in the hexagonal setting. (a) Outline of a unit cell containing one formula unit. (b) Projection of the Mn sublattice onto the *ab* plane with a slight *c*-axis component illustrating the corrugated Mn honeycomb lattice. Red arrows represent the magnetic moments at the Mn sites for $SrMn_2As_2$. Black lines show a unit cell.

In this paper we carried out ^{75}As nuclear magnetic resonance (NMR) measurements on trigonal $CaMn_2As_2$ and $SrMn_2As_2$ single crystals to investigate the static and dynamic magnetic properties from a microscopic point of view. Our NMR measurements clearly detected the AFM phase transitions at 62 and 120 K for $CaMn_2As_2$ and $SrMn_2As_2$, respectively. In the paramagnetic states, similar quadrupolar-split ^{75}As NMR spectra were observed in both compounds. However, quite different NMR spectra were detected in the AFM states. In $CaMn_2As_2$, broad and complex NMR spectra were observed in the AFM state, which clearly indicates a distribution of internal fields $B_{\rm int}$ at the As site. From the analysis of the spectra, the AFM state of $CaMn_2As_2$ was determined to be a two-dimensional incommensurate state where the Mn ordered moments are aligned in the *ab* plane. On the other hand, relatively sharp and distinct NMR lines were observed in the AFM state in $SrMn_2As_2$. The spectra indicate no obvious distribution of $B_{\rm int}$ in $SrMn_2As_2$. These results indicate that, contrary to $CaMn_2As_2$, the AFM state in $SrMn_2As_2$ is commensurate.

II. EXPERIMENT

The hexagonal-shaped single crystals of $CaMn_2As_2$ and $SrMn_2As_2$ for the NMR measurements were grown using Sn flux as reported in detail elsewhere [10]. NMR measurements were carried out on ^{75}As ($I = 3/2$, $\gamma/2\pi = 7.2919$ MHz/T, $Q = 0.29$ barns) using a homemade, phase-coherent, spin-echo pulse spectrometer. The ^{75}As NMR spectra were obtained by sweeping the magnetic field H at fixed frequencies $f = 51.1$, 9.1, and 53.1 MHz. The magnetic field was applied parallel to either the crystal *c* axis ($H \parallel c$) or to the *ab* plane ($H \parallel ab$). In this paper, when we use $H \parallel ab$, the magnetic field was applied along the edge direction of the hexagonal-shaped crystal corresponding to the *a* or *b* axes, except when we specify the direction in the *ab* plane for angle-dependent NMR spectrum measurements in the *ab* plane. The Tesla (T) is defined as 1 T $= 10^4$ Oe. The ^{75}As spin-lattice relaxation rate $1/T_1$ was measured with a saturation-recovery method. $1/T_1$ at each T was determined

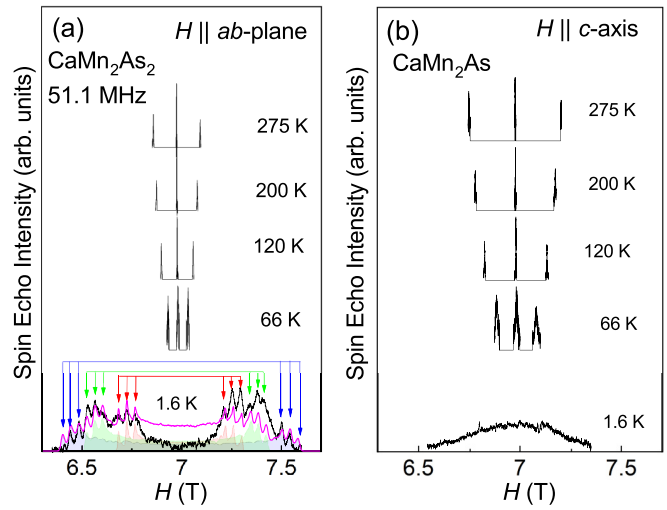

FIG. 2. Temperature variation of field-swept ^{75}As NMR spectra for a $CaMn_2As_2$ crystal at frequency $f = 51.1$ MHz for magnetic field directions (a) $H \parallel ab$ plane and (b) $H \parallel c$ axis in the paramagnetic and antiferromagnetic states. The spectra shown at the bottom in (a) and (b) were measured at 1.6 K. The arrows in three different colors in (a) show the splitting of the ^{75}As NMR spectra due to internal fields. The blue, green, and red areas are calculated NMR spectra based on the incommensurate AFM state for As1, As2, and As3 sites, respectively (see text). The magenta curve is the sum of the three calculated spectra.

by fitting the nuclear magnetization M versus time t using the exponential functions $1 - M(t)/M(\infty) = 0.1e^{-t/T_1} + 0.9e^{-6t/T_1}$ for ^{75}As NMR, where $M(t)$ and $M(\infty)$ are the nuclear magnetization at time t after the saturation and the equilibrium nuclear magnetization at $t \rightarrow \infty$, respectively.

III. RESULTS AND DISCUSSION

A. $CaMn_2As_2$

1. ^{75}As *NMR in the paramagnetic state*

Figures 2(a) and 2(b) show the field-swept ^{75}As NMR spectra of $CaMn_2As_2$ for two magnetic field directions, $H \parallel ab$ plane and $H \parallel c$ axis, respectively, measured at various temperatures. The typical spectrum for a nucleus with spin $I = 3/2$ with Zeeman and quadrupolar interactions can be described by the nuclear spin Hamiltonian [25], $\mathcal{H} = -\gamma_n\hbar(1+K)\mathbf{I}\cdot\mathbf{H} + \frac{h\nu_Q}{6}[3I_Z^2 - I^2 + \frac{1}{2}\eta(I_+^2 + I_-^2)]$, where $\mathbf{H}$ is external field, h is Planck's constant, and K represents the NMR shift. The nuclear quadrupole frequency for $I = 3/2$ nuclei is given by $\nu_Q = e^2QV_{ZZ}/2h$, where Q is the nuclear quadrupole moment, V_{ZZ} is the electric field gradient (EFG) at the As site, and η is the asymmetry parameter of the EFG defined by $\frac{V_{XX}-V_{YY}}{V_{ZZ}}$ with $|V_{ZZ}| \geqslant |V_{YY}| \geqslant |V_{XX}|$. In the case of $I = 3/2$, when the Zeeman interaction is much greater than the quadrupolar interaction, the NMR spectrum is composed of a central transition line ($I_z = 1/2 \leftrightarrow -1/2$) and a pair of satellite lines shifted from the central transition line by $\pm\frac{1}{2}\nu_Q(3\cos^2\theta - 1 + \eta\sin^2\theta\cos 2\phi)$ (for the transitions of $I_z = 3/2 \leftrightarrow 1/2$ and $-3/2 \leftrightarrow -1/2$) [26]. Here θ and ϕ are the polar and azimuthal angles between the principal Z axis of the EFG and the direction of $\mathbf{H}$, respectively. The observed

^{75}As NMR spectra of $CaMn_2As_2$ in the paramagnetic state can be well reproduced by calculations from the above simple Hamiltonian with $\eta = 0$ where the spectra for $H \parallel c$ and $H \parallel ab$ correspond to the case of $\theta = 0°$ and 90°, respectively. This indicates that the Z axis of the EFG at the As site is parallel to the c axis, consistent with the threefold rotational symmetry around the c axis at the As site.

The relatively sharp lines with the full width at half maximum (FWHM) of ∼20 and 17 Oe for $H \parallel c$ and $H \parallel ab$, respectively, for the central transition lines are nearly independent of temperature above 150 K, as shown in Fig. 3(a). Below 150 K, with decreasing temperature, the FWHM values start to increase gradually and rapidly increase below ∼70 K due to the AFM ordering at $T_N = 62$ K, indicating the second-order nature of the AFM phase transition in $CaMn_2As_2$.

Figure 3(b) shows the temperature dependence of the NMR shifts for $H \parallel c$ axis (K_c) and $H \parallel ab$ plane (K_{ab}) for $CaMn_2As_2$. For both directions, K decreases slightly with decreasing temperature from 300 K to T_N, consistent with the temperature dependence of the magnetic susceptibility [10], where a broad peak in χ was observed around $T = 400$ K. The temperature dependencies of K and χ indicate short-range AFM order in the paramagnetic state [10]. The NMR shift has contributions from the T-dependent spin part K_{spin} and a T-independent orbital part K_0. K_{spin} is proportional to the spin susceptibility χ_{spin} through the hyperfine coupling constant A giving $K(T) = K_0 + \frac{A}{N_A}\chi_{spin}(T)$, where N_A is Avogadro's number. The inset of Fig. 3(b) plots K_{ab} and K_c for $CaMn_2As_2$ against the corresponding χ_{ab} and χ_c, respectively, with T as an implicit parameter. All K_{ab} and K_c are seen to vary linearly with the corresponding χ, and the hyperfine coupling constants are estimated to be $A_c = (-2.10 \pm 0.03)$ T/μ_B, and $A_{ab} = (-1.66 \pm 0.04)$ T/μ_B for $H \parallel c$ and $H \parallel ab$, respectively.

From the spectra shown in Figs. 2(a) and 2(b), we also extracted the temperature dependence of ν_Q for $CaMn_2As_2$, which is shown in Fig. 3(c). ν_Q decreases from 1.70 MHz at $T = 275$ K to 0.70 MHz at 66 K. This is in contrast to the case of $SrMn_2As_2$ as will be shown below where ν_Q increases with decreasing temperature.

2. ^{75}As *NMR spectra in the antiferromagnetic state*

Below $T_N = 62$ K, the NMR lines broaden suddenly and the spectrum could not be measured in the AFM state due to poor signal intensity, except at the lowest temperature $T = 1.6$ K of our ^{4}He cryostat where we were able to measure the spectra although the signal intensities were still weak. As shown at the bottom in Fig. 2(b), a single broad spectrum without clear splitting is observed for $H \parallel c$. On the other hand, for $H \parallel ab$, the NMR spectrum splits into two main broad lines with multiple peaks in Fig. 2(a). From the analysis of the observed spectrum, we found that it can be explained by three As sites with lines split due to different internal fields as shown by arrows in Fig. 2(a). It is important to point out that each peak is asymmetric and tails toward the center of the spectrum, which cannot be explained by a commensurate AFM state. This asymmetric shape is reminiscent of a so-called two-dimensional powder pattern of NMR spectra which is expected for a planar incommensurate AFM state.

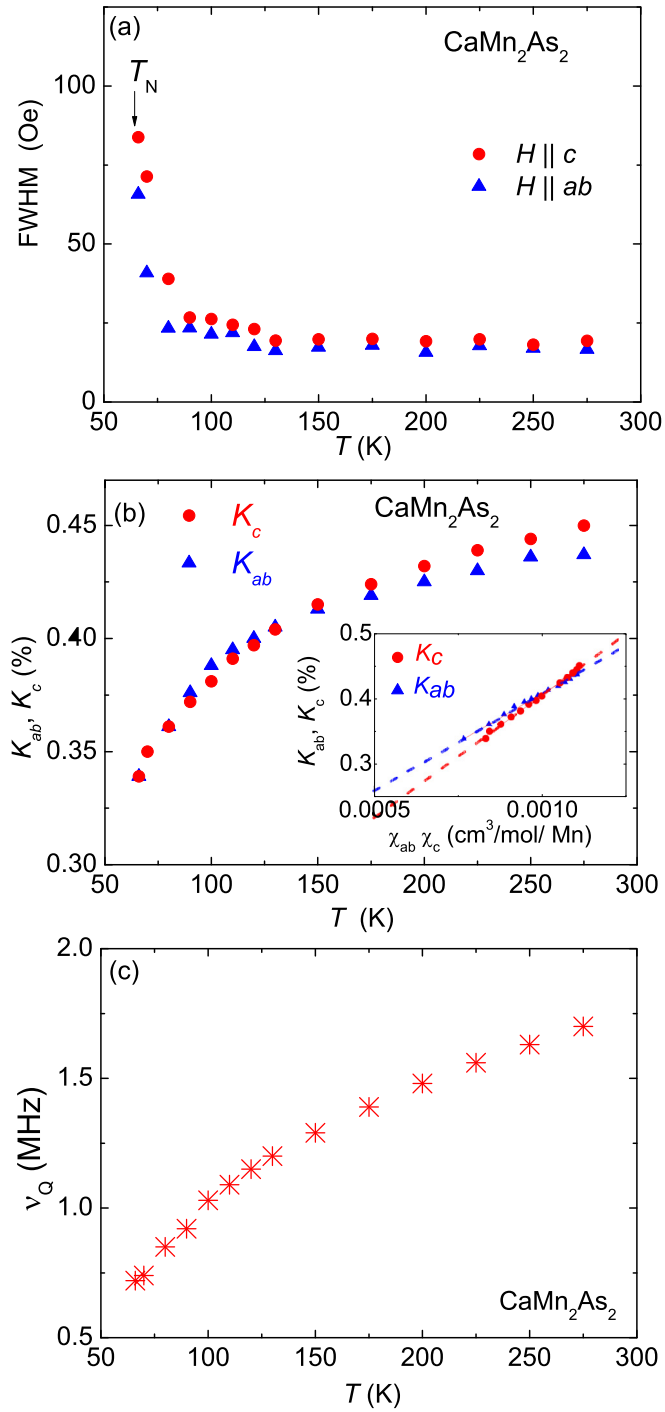

FIG. 3. (a) Temperature dependence of the full width at half maximum (FWHM) of the central transition lines for $H \parallel c$ and $H \parallel ab$. (b) Temperature dependence of the ^{75}As NMR shift for $H \parallel c$ axis (K_c) and $H \parallel ab$ plane (K_{ab}). Inset: K vs magnetic susceptibility χ for the corresponding ab and c components of K in $CaMn_2As_2$ with T as an implicit parameter. The dashed lines are linear fits. (c) Temperature dependence of the quadrupole frequency ν_Q for $CaMn_2As_2$.

Therefore, we calculated NMR spectra assuming a planar incommensurate AFM state. The result is shown by the magenta curves in Fig. 2(a). The calculated spectrum is a sum of three As NMR spectra with different internal fields (B_{int}) and ν_Q

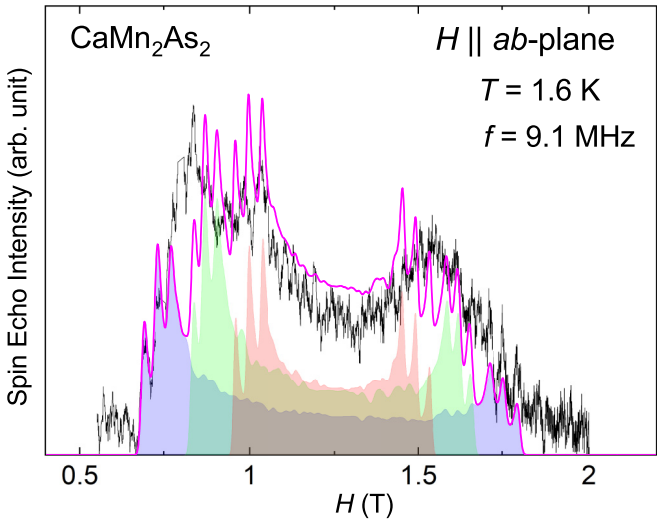

FIG. 4. Field-swept ^{75}As NMR spectrum measured at $T = 1.6$ K and $f = 9.1$ MHz for $H \parallel ab$ in the AFM state. The blue, green, and red areas are calculated NMR spectra based on the incommensurate AFM state for As1, As2, and As3 sites, respectively. Here the parameters of $B_{\rm int}$ and $\nu_{\rm Q}$ used are the same as those estimated from the spectrum measured at 51.1 MHz. The magenta curve is the sum of the three calculated spectra.

shown by three areas in different colors at the bottom of Fig. 2(a). Here we used $|B_{\rm int}| = 0.50$, 0.38, and 0.26 T and $\nu_{\rm Q} = 0.59$, 0.49, and 0.58 MHz for As sites denoted by As1, As2, and As3 shown in blue, green, and red, respectively. The characteristic shape of the observed spectrum can be roughly captured by the simulation, although the calculated signal intensity around the Larmor field is higher than observed. To check the external field dependence of the NMR spectrum, we measured the ^{75}As NMR spectrum at a different resonance frequency of 9.1 MHz for $H \parallel ab$ shown in Fig. 4. Similar to the case of $f = 51.1$ MHz, two broad lines with multiple peaks are observed. The magenta curve in the figure shows the calculated spectrum for the incommensurate AFM state with the same values of the parameters as for the $f = 51.1$ MHz. The calculated spectrum seems to reproduce the characteristic shape of the observed spectrum, suggesting the incommensurate AFM state in $CaMn_2As_2$.

In order to investigate the in-plane angle (ϕ) dependence of the internal field and the spacing of quadrupolar splitting, we measured the ϕ dependence of the ^{75}As NMR spectra at $f = 53.1$ MHz and $T = 1.6$ K (Fig. 5). It is clear that the spectrum slightly changes by changing ϕ due to a change in $B_{\rm int}$ and in the quadrupolar splittings, although all the spectra keep showing the asymmetric shape.

Figures 6(a) and 6(b) show the ϕ dependence of $B_{\rm int}$ and quadrupolar splitting for three different As sites estimated from the spectra, respectively. According to the neutron-diffraction measurements on the antiferromagnetic state of $SrMn_2As_2$ [24], the AFM state is collinear with the ordered Mn moments aligned in the *ab* plane where three AFM domains with their axes at 60° to each other exist within the *ab* plane. Assuming the three-domain collinear scenario in $CaMn_2As_2$, the component of $B_{\rm int}$ parallel to the external field should change as a function of the cosine of ϕ. As shown

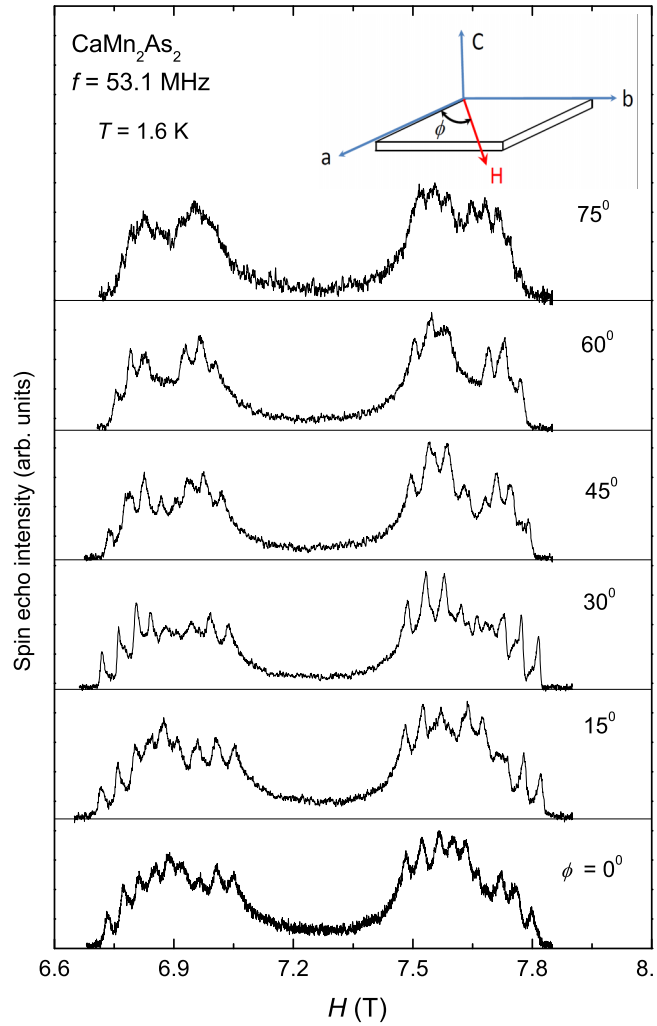

FIG. 5. In-plane angle (ϕ) dependence of field-swept ^{75}As NMR spectra of $CaMn_2As_2$ for $H \parallel ab$ plane measured at $f = 53.1$ MHz and $T = 1.6$ K in the antiferromagnetic state.

in Fig. 6(a), the $B_{\rm int}$ values slightly depend on ϕ, but the ϕ dependence does not follow the relation expected from the three-domain collinear scenario. Thus this scenario can be excluded. The small ϕ dependence of $B_{\rm int}$ could be explained by introducing an anisotropy in the hyperfine field in the *ab* plane.

As for the ϕ dependence of quadrupolar splittings, one does not expect any angle dependence for the three-domain scenario since the As site for each domain is expected to have $\eta = 0$. This is inconsistent with the experimental observation. In order to change the quadrupolar spacing in the *ab* plane, one needs to have η finite, suggesting a change in the local symmetry at the As sites. This suggests a change in the crystal structure in the AFM state, which may produce the three different As sites with different $B_{\rm int}$ and $\nu_{\rm Q}$. It is noted that a broad peak of the spectrum ($H \parallel c$) centered around the Larmor field would be consistent with the incommensurate AFM state if the internal fields are anisotropic in the *ab* plane. Therefore, we conclude that the AFM state of $CaMn_2As_2$ is not commensurate but incommensurate where the ordered Mn moments are most likely in the *ab* plane. However, the

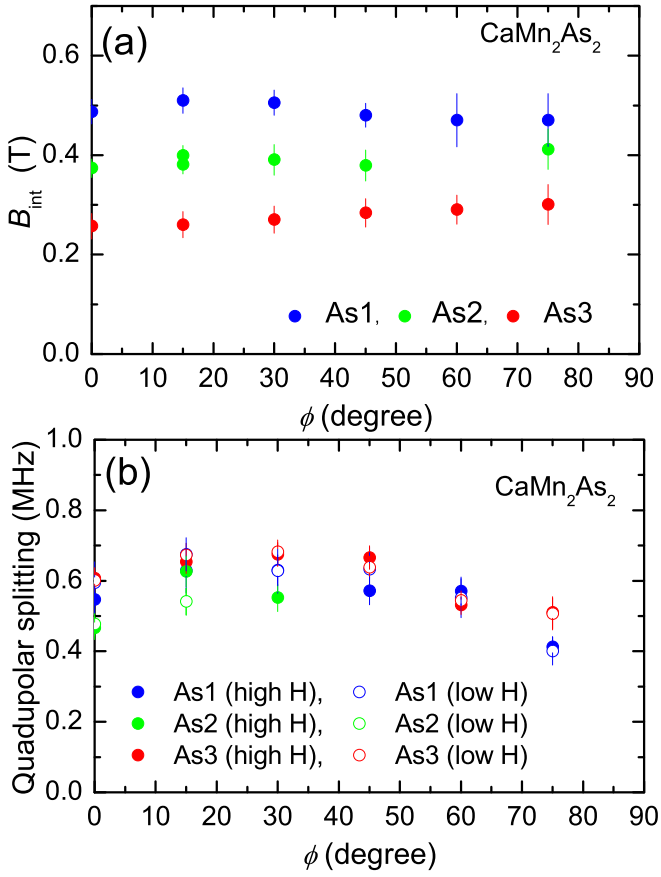

FIG. 6. (a) ϕ dependence of $B_{\rm int}$ for three different As sites (As1 in blue, As2 in green, and As3 in red) in $CaMn_2As_2$. (b) ϕ dependence of quadrupolar splitting estimated from the spacing between the lines for the As1, As2, and As3 sites. The open and solid symbols represent the quadrupolar splitting for each As site in the lower H (low H) and higher H (high H) peaks, respectively.

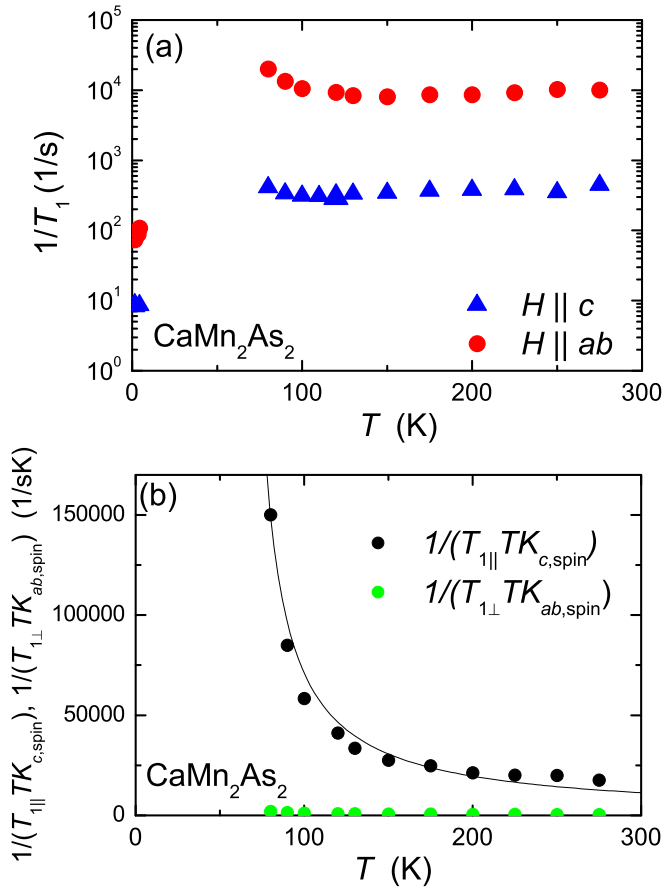

FIG. 7. (a) Temperature dependence of ^{75}As spin-lattice relaxation rates $1/T_1$ in $CaMn_2As_2$ for $H \parallel c$ axis and $H \parallel ab$ plane. (b) Temperature dependence of $1/T_{1,\perp}TK_{ab,\rm spin}$ and $1/T_{1,\parallel}TK_{c,\rm spin}$ for $CaMn_2As_2$. The black curve is the Curie-Weiss fit of $C/(T-\theta)$ with $C = 2.7 \times 10^6$ s^{-1} and $\theta = 62$ K.

linewidth of the spectrum is much greater than expected from the estimated $B_{\rm int}$. It is also noted that no clear quadrupolar splitting of the line is observed in the spectrum for $H \parallel c$ in the AFM state. These results indicate a large distribution of $B_{\rm int}$ along the c axis and, thus, a more complicated magnetic structure; however, the reason for the distribution is not clear at present. Further studies such as neutron-diffraction measurements are required to determine the magnetic structure of $CaMn_2As_2$ in detail.

3. ^{75}As *spin-lattice relaxation rate* $1/T_1$

To investigate the spin dynamics, we have measured the ^{75}As spin-lattice relaxation rate $1/T_1$ as a function of temperature. Figure 7(a) shows the temperature dependence of $1/T_1$ in $CaMn_2As_2$ for $H \parallel c$ axis and $H \parallel ab$ plane. $1/T_1$ shows a very large anisotropy in the paramagnetic state where $1/T_1$ for $H \parallel ab$ is more than one order of magnitude greater than that for $H \parallel c$.

In order to analyze the spin fluctuation effects in the paramagnetic state above 62 K, it is useful to plot the data by changing the vertical axis from $1/T_1$ to $1/T_1TK_{\rm spin}$. In general, $\frac{1}{T_1T}$ is expressed in terms of the dynamical susceptibility $\chi(\vec{q},\omega_0)$ per mole of electronic spins as $\frac{1}{T_1T} = \frac{2\gamma_N^2 k_B}{N_A^2}\sum_{\vec{q}} |A(\vec{q})|^2 \frac{\chi''(\vec{q},\omega_0)}{\omega_0}$, where γ_N is the nuclear gyromagnetic ratio, k_B is Boltzmann's constant, N_A is Avogadro's number, the sum is over wave vectors $\vec{q}$ within the first Brillouin zone, $A(\vec{q})$ is the form factor of the hyperfine interactions as a function of $\vec{q}$, and $\chi''(\vec{q},\omega_0)$ is the imaginary part of the dynamical susceptibility at the nuclear Larmor angular frequency ω_0. On the other hand, $K_{\rm spin}$ is proportional to the uniform static susceptibility $\chi = \chi'(0,0)$, which is the real component of $\chi'(\vec{q},\omega_0)$ with $q = 0$ and $\omega_0 = 0$. Thus a plot of $1/T_1TK_{\rm spin}$ versus T shows the T dependence of $\sum_{\vec{q}}|A(\vec{q})|^2\chi''(\vec{q},\omega_0)$ with respect to that of the uniform susceptibility $\chi'(0,0)$.

To proceed with the analysis, one needs to take the anisotropy of $K_{\rm spin}$ and $1/T_1T$ into consideration. Since $1/T_1T$ probes magnetic fluctuations perpendicular to the magnetic field, it is natural to consider $1/T_{1,\perp}T \equiv 1/(T_1T)_{H\|c}$ when examining the character of spin fluctuations in the ab plane. Similarly, we consider $1/(T_{1,\parallel}T) = 2/(T_1T)_{H\|ab} - 1/(T_1T)_{H\|c}$ for spin fluctuations along the c axis. Strictly speaking, this simple relation is not applicable if $1/T_1T$ has a strong anisotropy in the ab plane. However, since $1/T_{1,\parallel}T$ is much greater than $1/T_{1,\perp}T$, one can still ap-

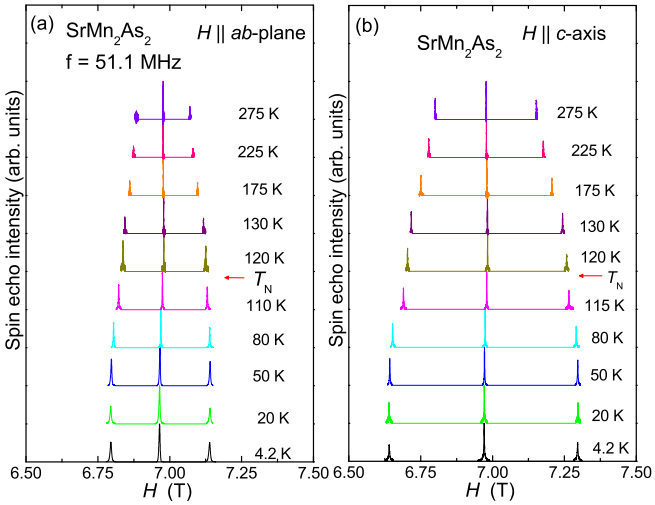

FIG. 8. Temperature variation of field-swept ^{75}As NMR spectra for a $SrMn_2As_2$ crystal at $f = 51.1$ MHz for the two magnetic field directions, (a) $H \parallel ab$ plane and (b) $H \parallel c$ axis.

ply the relation. Figure 7(b) shows the T dependence of $1/T_{1\parallel}TK_{c,\mathrm{spin}}$ and $1/T_{1\perp}TK_{ab,\mathrm{spin}}$. $1/T_{1\parallel}TK_{c,\mathrm{spin}}$ is much greater than $1/T_{1\perp}TK_{ab,\mathrm{spin}}$, indicating that hyperfine-field fluctuations at the As site along the c axis are much greater than that in the ab plane. $1/T_{1\parallel}TK_{c,\mathrm{spin}}$ increases with decreasing temperature. This clearly implies $\sum_{\vec{q}}|A(\vec{q})|^2\chi''(\vec{q},\omega_0)$ increases more than $\chi'(0,0)$, which is due to a growth of spin fluctuations with $q \neq 0$, most likely with AFM wave vector $q = Q_{\mathrm{AF}}$, even at T much higher than T_{N}. Thus we conclude that strong AFM spin fluctuations are realized in a wide temperature region up to at least ~300 K in the paramagnetic state, as has been pointed out from χ measurements [10]. In addition, the fact that $1/T_{1\parallel}TK_{c,\mathrm{spin}}$ is much greater than $1/T_{1\perp}TK_{ab,\mathrm{spin}}$ indicates that the AFM spin fluctuations are highly anisotropic in $CaMn_2As_2$. The enhancement of $1/T_{1\parallel}TK_{c,\mathrm{spin}}$ can be reproduced by a Curie-Weiss formula of $C/(T-\theta)$ with $C = 2.7 \times 10^6$ s^{-1} and $\theta = 62$ K as shown by the solid curve in Fig. 7(b). Since a Curie-Weiss behavior of $1/T_1T$ is expected for AFM spin fluctuations for a two-dimensional system from the self-consistent renormalization theory [27], our results suggest a two-dimensional nature of the AFM spin fluctuations in $CaMn_2As_2$.

B. $SrMn_2As_2$

1. ^{75}As *NMR spectra in the paramagnetic state*

Figures 8(a) and 8(b) show the temperature dependencies of the field-swept ^{75}As NMR spectra of $SrMn_2As_2$ for $H \parallel c$ and $H \parallel ab$. Similar to the case of $CaMn_2As_2$, clear quadrupolar-split lines were observed, but the observed lines are slightly sharper than those in $CaMn_2As_2$.

The FWHM of the central transition line at $T = 275$ K for $H \parallel c$ and $H \parallel ab$ is ~10 and 8 Oe, respectively, and their temperature dependencies are shown in Fig. 9(a). The principal axis of the EFG at the As site in $SrMn_2As_2$ is determined to be the c axis as in $CaMn_2As_2$, as expected because of the same crystal structure. Figure 9(b) shows the temperatures dependencies of K_c and K_{ab}. K_c and K_{ab} decrease slightly with

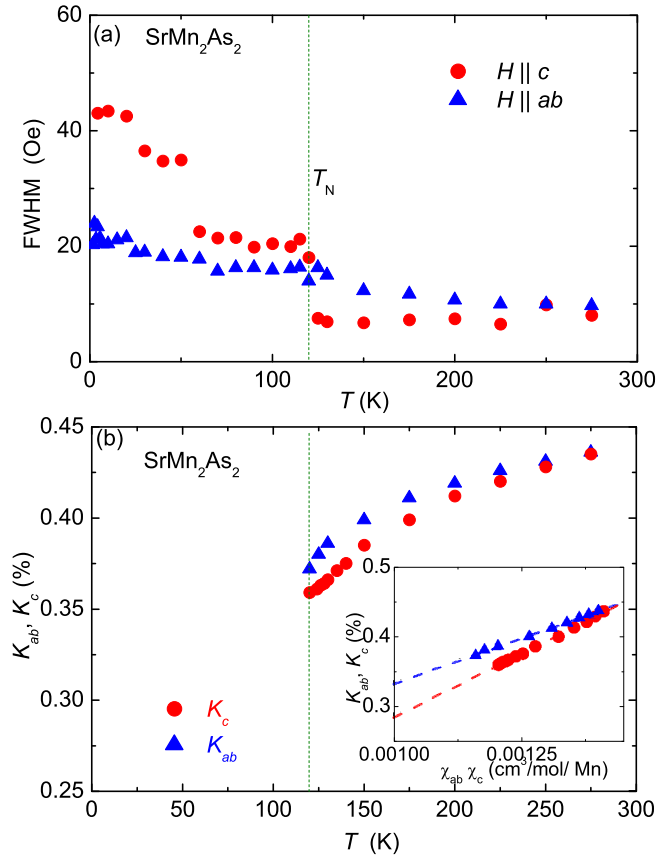

FIG. 9. (a) The FWHM of the central transition lines for $H \parallel c$ and $H \parallel ab$ for $SrMn_2As_2$. The vertical dashed line indicates $T_{\mathrm{N}} = 120$ K. (b) Temperature dependence of ^{75}As NMR shift K_c and K_{ab} for $H \parallel c$ axis and $H \parallel ab$ plane, respectively. Inset: K vs magnetic susceptibility χ for the corresponding ab and c components of K in $SrMn_2As_2$ with T as an implicit parameter. The dashed lines are linear fits.

decreasing temperature down to T_{N}. The inset of Fig. 9(b) plots K_{ab} and K_c against the corresponding χ_{ab} and χ_c, respectively, for $SrMn_2As_2$ with T as an implicit parameter. All K_{ab} and K_c are seen to vary linearly with the corresponding χ, and the hyperfine coupling constants are estimated to be $A_c = (-2.02 \pm 0.02)$ T/μ_{B}, and $A_{ab} = (-1.44 \pm 0.03)$ T/μ_{B}.

Figure 10(a) shows the temperature dependence of ν_{Q} for $SrMn_2As_2$ extracted from the spectra. ν_{Q} for $SrMn_2As_2$ increases from 1.30 MHz at $T = 275$ K to 2.40 MHz at 50 K, and levels off at low temperatures with an obvious change of the slope at T_{N} from concave to convex shape with decreasing temperature. The T dependence is opposite to the case of $CaMn_2As_2$ in Fig. 3(c). Since ν_{Q} generally depends on the lattice constants in insulators, the results suggest an opposite temperature dependence of the lattice constants in the two compounds.

2. ^{75}As *NMR spectra in the antiferromagnetic state*

Different from the ^{75}As NMR spectra of $CaMn_2As_2$ in Fig. 2, each line of the spectra in $SrMn_2As_2$ shifts to lower fields without showing any splitting for both $H \parallel c$ and $H \parallel ab$ in the AFM state below $T_{\mathrm{N}} = 120$ K, as shown in Figs. 8(a)

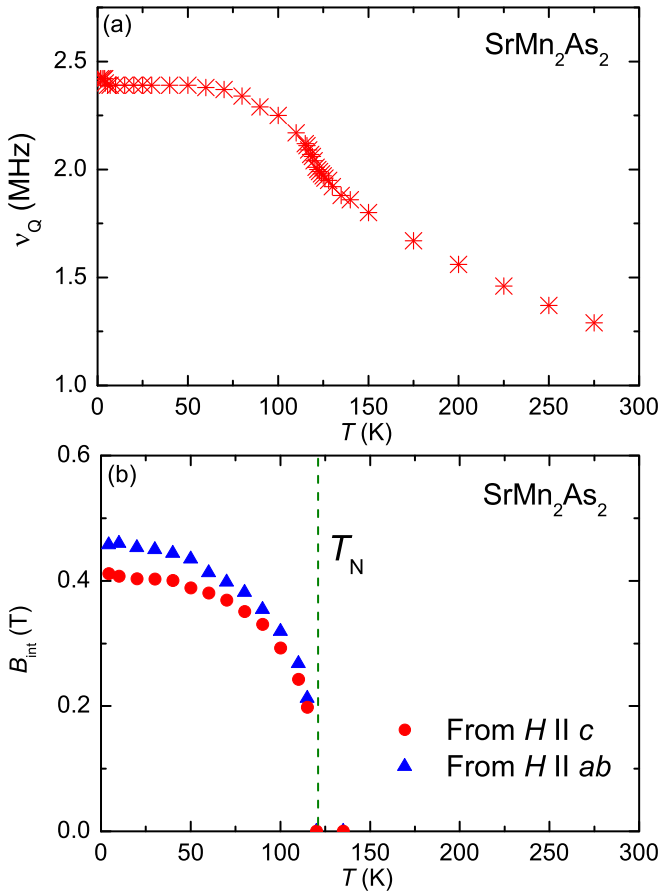

FIG. 10. (a) Temperature dependence of quadrupole frequency ν_Q for $SrMn_2As_2$. (b) Temperature dependence of the internal field B_{int} at the As nuclei associated with the antiferromagnetic order in $SrMn_2As_2$. The vertical dashed line indicates T_N.

and 8(b). Although each line broadens slightly, the observed spectra are much sharper than those observed in $CaMn_2As_2$ in the AFM state as described above. The distinct NMR lines below T_N clearly indicate that the AFM state is commensurate, which is in strong contrast to the incommensurate AFM state in $CaMn_2As_2$.

A lack of splitting of the NMR lines indicates that the unique internal field at the As site is perpendicular to the external field direction. When $B_{int} \perp H$, the effective field B_{eff} at the As site is given by $B_{eff} = \sqrt{H^2 + {B_{int}}^2}$. Figure 10(b) shows the temperature dependence of the estimated B_{int} using the above formula based on the observed spectra for both H directions below T_N. The temperature dependencies of B_{int} clearly indicate a second-order AFM phase transition in $SrMn_2As_2$. B_{int} around 0.4–0.5 T in $SrMn_2As_2$ at low temperatures seems to be comparable to values in $CaMn_2As_2$.

We do not observe any evidence for the AFM three domains proposed by the neutron-diffraction measurements. This is due to the application of a large magnetic field of 7 T which causes the ordered Mn moments in the three domains to point perpendicular to the external field direction, making them indistinguishable from NMR spectrum measurements. According to the magnetization measurements [10], one needs to perform NMR spectrum measurements at least below 0.5 T to test the three-domain scenario which would be difficult to perform due to the signal intensity issue as well as the comparable values of B_{int} and H.

Finally it is interesting to note that, since we observe only one As site, no structural phase transition is expected in $SrMn_2As_2$, while a possible structural distortion in $CaMn_2As_2$ was suggested above because of the observation of at least three As sites with finite η in the AFM state. According to theoretical studies on hexagonal antiferromagnets [15–17], various magnetic phases are proposed due to a competition between first-, second-, and third-neighbor magnetic exchange interactions J_1, J_2, and J_3, respectively, between the Mn moments on the hexagonal lattice. For classical localized spins described by a Heisenberg Hamiltonian, Néel, stripy, zigzag, and spiral magnetic orderings are possible depending on the relative strengths of these interactions [15–17]. We infer that the possible structural transition in $CaMn_2As_2$ makes a change in the relative strengths of the exchange interactions, resulting in an incommensurate AFM state, different from the commensurate collinear AFM state in $SrMn_2As_2$. It is also noted that the two systems (Sr, Ca)Mn_2As_2 exhibit different magnetocrystalline anisotropies although the valence states of the Mn^{2+} ($S = 5/2$) ions are similar, which may also originate from the different crystal structures suggested by the present NMR measurements.

3. ^{75}As *spin-lattice relaxation rates*

Figure 11(a) shows the temperature dependence of $1/T_1$ in $SrMn_2As_2$ for $H \parallel c$ axis and $H \parallel ab$ plane. In the paramagnetic state, $1/T_1$ shows a large anisotropy, where $1/T_1$ for $H \parallel ab$ is larger than that for $H \parallel c$, and an enhancement of $1/T_1$ with decreasing temperature is observed only for $H \parallel ab$, similar to that in $CaMn_2As_2$. Below T_N, $1/T_1$ shows a strong T dependence for T above 20 K, where $1/T_1$ shows a T^5 power-law behavior (shown by the green dashed lines in the figure). This power-law T dependence of $1/T_1$ can be explained by a three-magnon process as the main relaxation mechanism for an AFM insulating state when $T \gg \Delta$, where Δ is the anisotropy gap energy in the spin wave spectrum [28]. A deviation from power-law behavior below 20 K was observed and $1/T_1$ shows a broad maximum. This feature at low temperatures is likely due to relaxation associated with impurities.

As in the case of $CaMn_2As_2$, we evaluated two quantities, $1/T_{1\parallel}TK_{c,spin}$ and $1/T_{1,\perp}TK_{ab,spin}$, for $SrMn_2As_2$ with the same procedure described above, whose temperature dependencies are shown in Fig. 11(b). Similar to the case of $CaMn_2As_2$, a clear and strong enhancement of $1/T_{1\parallel}TK_{c,spin}$ is also observed originating from the AFM spin fluctuations in the paramagnetic state in $SrMn_2As_2$. The AFM spin fluctuations are also characterized by a two-dimensional nature as the temperature dependence of $1/T_{1\parallel}TK_{c,spin}$ is well described by a Curie-Weiss behavior shown by the solid line in Fig. 11(b), as in $CaMn_2As_2$.

IV. SUMMARY

In summary, we have found different antiferromagnetic spin structures in $CaMn_2As_2$ and $SrMn_2As_2$ from ^{75}As NMR

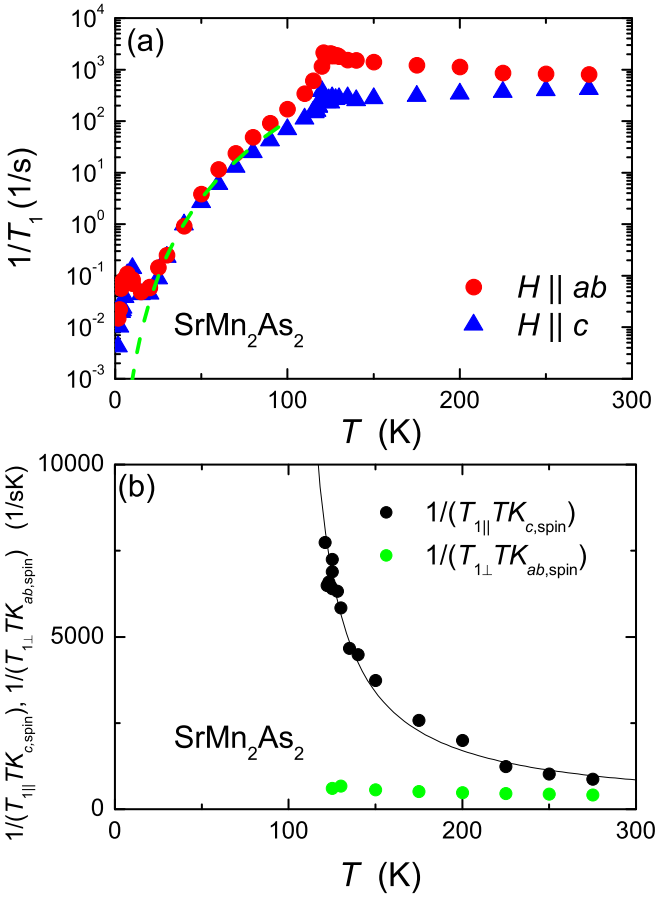

FIG. 11. (a) Temperature dependence of the ^{75}As spin-lattice relaxation rates $1/T_1$ in $SrMn_2As_2$ for $H \parallel c$ axis and $H \parallel ab$ plane. The light green dashed line shows a $1/T_1 \propto T^5$ power-law behavior. (b) Temperature dependence of $1/T_{1,\parallel} TK_{c,spin}$ and $1/T_{1,\perp} TK_{ab,spin}$. The black curve is the Curie-Weiss fit of $C/(T-\theta)$ with $C = 1.7 \times 10^5$ s^{-1} and $\theta = 100$ K.

measurements performed on single crystals. In $SrMn_2As_2$, relatively sharp and distinct ^{75}As NMR lines were observed and the NMR spectra were shifted to lower fields for both $H \parallel c$ axis and $H \parallel ab$ plane, suggesting that the internal field B_{int} produced by the Mn ordered moments is nearly perpendicular to the external magnetic field direction. No obvious distribution of the internal field B_{int} was observed in $SrMn_2As_2$, which clearly indicates a commensurate AFM state. In sharp contrast, broad and complex NMR spectra were observed in $CaMn_2As_2$ in the AFM state, which clearly shows a distribution of B_{int} at the As site, thus indicating an incommensurate state. From the analysis of the characteristic shape of the observed spectra, the AFM state of $CaMn_2As_2$ was determined to be a two-dimensional incommensurate state where Mn ordered moments are aligned in the *ab* plane. A possible origin of the incommensurate AFM state in $CaMn_2As_2$ was suggested to be a structure distortion, which may result in changing the relative strengths of the exchange interactions.

Quite recently, the isostructural phosphorus-based antiferromagnetic compounds $SrMn_2P_2$ ($T_N = 53$ K) and $CaMn_2P_2$ ($T_N = 69.8$ K) were reported to show weak and strong first-order AFM transitions, respectively [7]. This is different from the second-order nature of the AFM transitions observed in the arsenic-based compounds $SrMn_2As_2$ and $CaMn_2As_2$ studied here. It is also interesting to point out that the AFM structure of $CaMn_2P_2$ is suggested to be commensurate and that of $SrMn_2P_2$ to be incommensurate [7], in contrast to the present compounds (incommensurate in $CaMn_2As_2$ and commensurate in $SrMn_2As_2$). It is important to understand the origin of the different nature of AFM phase transitions such as the order of the phase transition as well as the commensurate or incommensurate nature in those compounds. Our results encourage further experimental and theoretical studies to identify the origins of these features in the Mn compounds.

ACKNOWLEDGMENTS

The research was supported by the U.S. Department of Energy, Office of Basic Energy Sciences, Division of Materials Sciences and Engineering. Ames Laboratory is operated for the U.S. Department of Energy by Iowa State University under Contract No. DE-AC02-07CH11358.

[1] Y. Kamihara, T. Watanabe, M. Hirano, and H. Hosono, Iron-based layered superconductor La[$O_{1-x}F_x$]FeAs (x = 0.05-0.12) with $T_c = 26$ K, J. Am. Chem. Soc. **130**, 3296 (2008).

[2] D. C. Johnston, The puzzle of high temperature superconductivity in layered iron pnictides and chalcogenides, Adv. Phys. **59**, 803 (2010).

[3] P. C. Canfield and S. L. Bud'ko, FeAs-based superconductivity: A case study of the effects of transition metal doping on $BaFe_2As_2$, Annu. Rev. Condens. Matter Phys. **1**, 27 (2010).

[4] G. R. Stewart, Superconductivity in iron compounds, Rev. Mod. Phys. **83**, 1589 (2011).

[5] Y. Singh, M. A. Green, Q. Huang, A. Kreyssig, R. J. McQueeney, D. C. Johnston, and A. I. Goldman, Magnetic order in $BaMn_2As_2$ from neutron diffraction measurements, Phys. Rev. B **80**, 100403(R) (2009).

[6] A. Mewis, AB_2X_2-Compounds with the $CaAl_2Si_2$ Structure, V[1] The crystal structure of $CaMn_2P_2$, $CaMn_2As_2$, $SrMn_2P_2$, and $SrMn_2As_2$, Z. Naturforsch. B **33**, 606 (1978).

[7] N. S. Sangeetha, S. Pakhira, Q.-P. Ding, L. Krause, H.-C. Lee, V. Smetana, A.-V. Mudring, B. B. Iversen, Y. Furukawa, and D. C. Johnston, First-order antiferromagnetic transitions of $SrMn_2P_2$ and $CaMn_2P_2$ single crystals containing corrugated-honeycomb Mn sublattices, Proc. Natl. Acad. Sci. U.S.A. **118**, e2108724118 (2021).

[8] E. Brechtel, G. Cordier, and H. Schäfer, New ternary alkaline earth compounds of arsenic with manganese, Z. Naturforsch. B **33**, 820 (1978).

[9] Z. W. Wang, H. X. Yang, H. F. Tian, H. L. Shi, J. B. Lu, Y. B. Qin, Z. Wang, and J. Q. Li, Structural and physical properties of $SrMn_2As_2$, J. Phys. Chem. Solids **72**, 457 (2011).

[10] N. S. Sangeetha, A. Pandey, Z. A. Benson, and D. C. Johnston, Strong magnetic correlations to 900 K in single crystals of the trigonal antiferromagnetic insulators $SrMn_2As_2$ and $CaMn_2As_2$, Phys. Rev. B **94**, 094417 (2016).

[11] N. S. Sangeetha, V. Smetana, A.-V. Mudring, and D. C. Johnston, Antiferromagnetism in semiconducting $SrMn_2Sb_2$ and $CaMn_2Sb_2$ single crystals, Phys. Rev. B **97**, 014402 (2018).

[12] W. Ratcliff II, A. L. Lima Sharma, A. M. Gomes, J. L. Gonzalez, Q. Huang, and J. Singleton, The magnetic ground state of $CaMn_2Sb_2$, J. Magn. Magn. Mater. **321**, 2612 (2009).

[13] C. A. Bridges, V. V. Krishnamurthy, S. Poulton, M. P. Paranthaman, B. C. Sales, C. Myers, and S. Bobev, Magnetic order in $CaMn_2Sb_2$ studied via powder neutron diffraction, J. Magn. Magn. Mater. **321**, 3653 (2009).

[14] Q. D. Gibson, H. Wu, T. Liang, M. N. Ali, N. P. Ong, Q. Huang, and R. J. Cava, Magnetic and electronic properties of $CaMn_2Bi_2$: A possible hybridization gap semiconductor, Phys. Rev. B **91**, 085128 (2015).

[15] E. Rastelli, A. Tassi, and L. Reatto, Non-simple magnetic order for simple Hamiltonians, Physica B+C **97**, 1 (1979).

[16] I. I. Mazin, $CaMn_2Sb_2$: A fully frustrated classical magnetic system, arXiv:1309.3744.

[17] D. E. McNally, J. W. Simonson, J. J. Kistner-Morris, G. J. Smith, J. E. Hassinger, L. DeBeer-Schmidt, A. I. Kolesnikov, I. A. Zaliznyak, and M. C. Aronson, $CaMn_2Sb_2$: Spin waves on a frustrated antiferromagnetic honeycomb lattice, Phys. Rev. B **91**, 180407(R) (2015).

[18] J. B. Fouet, P. Sindzingre, and C. Lhuillier, An investigation of the quantum J_1-J_2-J_3 model on the honeycomb lattice, Eur. Phys. J. B **20**, 241 (2001).

[19] J. Zeng, S. Qin, C. Le, and J. Hu, Magnetism and superconductivity in the layered hexagonal transition metal pnictides, Phys. Rev. B **96**, 174506 (2017).

[20] D. C. Johnston, Magnetic Susceptibility of Collinear and Noncollinear Heisenberg Antiferromagnets, Phys. Rev. Lett. **109**, 077201 (2012).

[21] D. C. Johnston, Unified molecular field theory for collinear and noncollinear Heisenberg antiferromagnets, Phys. Rev. B **91**, 064427 (2015).

[22] V. K. Anand and D. C. Johnston, Antiferromagnetism in $EuCu_2As_2$ and $EuCu_{1.82}Sb_2$ single crystals, Phys. Rev. B **91**, 184403 (2015).

[23] D. H. Ryan, J. M. Cadogan, V. K. Anand, D. C. Johnston, and R. Flacau, The magnetic structure of $EuCu_2Sb_2$, J. Phys.: Condens. Matter **27**, 206002 (2015).

[24] P. Das, N. S. Sangeetha, A. Pandey, Z. A. Benson, T. W. Heitmann, D. C. Johnston, A. I. Goldman, and A. Kreyssig, Collinear antiferromagnetism in trigonal $SrMn_2As_2$ revealed by single-crystal neutron diffraction, J. Phys.: Condens. Matter **29**, 035802 (2017).

[25] C. P. Slichter, *Principles of Magnetic Resonance*, 3rd ed. (Springer, New York, 1990).

[26] A. Abragam, *The Principles of Nuclear Magnetism* (Clarendon Press, Oxford, 1961).

[27] T. Moriya, The effect of electron-electron interaction on the nuclear spin relaxation in metals, J. Phys. Soc. Jpn. **18**, 516 (1963).

[28] D. Beeman and P. Pincus, Nuclear spin-lattice relaxation in magnetic insulators, Phys. Rev. **166**, 359 (1968).